Materials Research Bulletin 95 (2017) 129–137

Contents lists available at ScienceDirect

Materials Research Bulletin

journal homepage: www.elsevier.com/locate/matresbu

Temperature-dependent selective growth of carbon nanotubes in Si/SiO_2 structures for field emitter array applications

Yu Dian Lim[a,*], Liangxing Hu[b], Alexander Vasiliyvich Avramchuck[c], Dmitry Grapov[c], Beng Kang Tay[a], Sheel Aditya[a], Jianmin Miao[b], Vladimir Labunov[c]

[a] School of Electrical and Electronics Engineering, Nanyang Technological University, 639798, Singapore
[b] School of Mechanical and Aerospace Engineering, Nanyang Technological University, 639798, Singapore
[c] Micro- and Nanoelectronics Department, Belarusian State University of Informatics and Radioelectronics, Minsk, 220013, Belarus

ARTICLE INFO

Article history:
Received 27 February 2017
Received in revised form 20 June 2017
Accepted 18 July 2017
Available online 23 July 2017

Keywords:
A. Nanostructures
B. Vapor deposition
B. Microstructure
C. Electron microscopy
D. Electrical properties

ABSTRACT

Temperature-dependent selective growth of Carbon Nanotubes (CNTs) in Si/SiO_2 structures using ferrocene/xylene volatile catalyst source and its application in Field Emitter Array (FEA) is demonstrated in this work. CNTs are grown directly on Si/SiO_2 substrates by volatile catalyst source (Ferrocene/Xylene) Chemical Vapor Deposition (CVD) technique and the effect of growth temperatures (760–880 °C) on CNT height and crystallinity has been studied. Selective growth of CNTs on Si substrates is achieved at 790 °C growth temperature. Using the obtained selective growth condition, CNT FEAs are fabricated by growing CNT bundles selectively on the Si surface of the pre-fabricated SiO_2 pits on a Si wafer. Field emission current density above 100 mA/cm^2 is obtained from inter-pit separation distances of 4–10 μm. These results show the potential of ferrocene/xylene catalyst source in achieving selective growth of CNTs in Si/SiO_2 structures for FEA application.

© 2017 Elsevier Ltd. All rights reserved.

1. Introduction

As predicted by Moore's law, there has been an exponential increase in the number of components fabricated on a commercial semiconductor chip over the past few decades [1]. Along with this progression, several technical issues have arisen, including off-leakage increase and drain current degradation [2]. To resolve these technical issues, it has been proposed by NASA to use vacuum electronic devices as a possibly better alternative as compared to the conventional Silicon (Si)-based solid-state electronic devices [3]. In general, vacuum electronic devices possess higher electron mobility, thermal durability and wider operational frequency range as compared to solid-state devices. However, vacuum electronic devices are heavier and bulkier than solid-state devices, which limits their applications in modern electronic systems [4]. In the proposal made by NASA, a possible strategy to miniaturize vacuum electronic devices has also been suggested, which includes integration of Si based microfabrication techniques in the fabrication process of vacuum electronic devices [3].

To enable the microfabrication of vacuum electronic devices, miniaturized, high current density field emitters with high growth selectivity are required. Various 1D nanostructure field emitters have been reported in the state-of-the-art, such as diamond nanowire [5], ZnO nanowire [6], silver nanowire [7], Carbon Nanotubes (CNTs) [8] *etc.* These nanostructures show promising Field Emission (FE) characteristics for possible application in modern vacuum electronic devices. Among the reported nanostructures, Carbon Nanotubes (CNTs) show outstanding FE properties resulting from their unique atomic structure [8]. A typical CNT Field Emitter Array (FEA) can be fabricated on a pre-deposited catalyst pattern (Ni, Fe, Co, *etc.*) via Chemical Vapour Deposition (CVD) technique [9]. By using this technique, CNTs can be grown selectively on the pre-patterned catalyst layer. Besides pre-patterned catalyst technique, a simpler approach to fabricate CNT FEA is the *in-situ* volatile catalyst source (ferrocene/xylene) CVD technique [10]. Due to the organometallic (Fe-hydrocarbon) nature of ferrocene, the Fe content in ferrocene can act as a catalyst for CNT growth without the presence of an external catalyst layer. Zhang et al. [11] have reported CNT growth on pristine Si substrates using volatile catalyst source technique. From the reported study, CNT growth is initiated by the formation of a continuous iron silicide barrier layer on the silicon substrate; the iron silicide is postulated to reduce the contact resistance between CNTs and the Si substrate. In addition to growth of CNTs using ferrocene/xylene catalyst, to successfully integrate ferrocene-grown CNTs in FEA

* Corresponding author.
E-mail address: limy0222@ntu.edu.sg (Y.D. Lim).

http://dx.doi.org/10.1016/j.materresbull.2017.07.022
0025-5408/© 2017 Elsevier Ltd. All rights reserved.

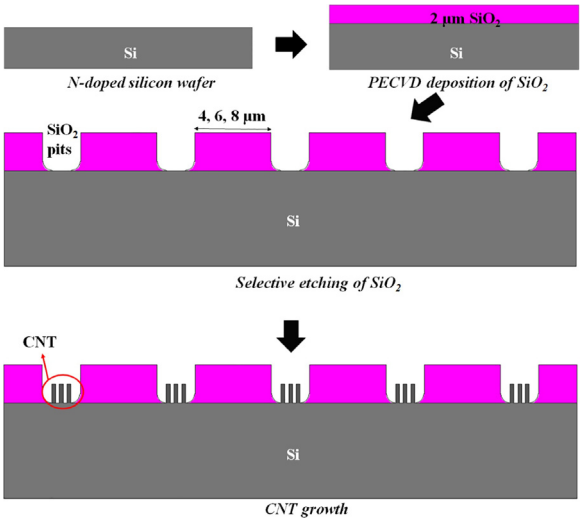

Fig. 1. Schematic diagram of CNTs grown in Si/SiO_2 structure.

applications, selective growth of CNTs in Si/SiO_2 structures is crucial. Jung et al. have reported selective growth of CNTs in Si/SiO_2 structures on the SiO_2 surfaces using volatile catalyst technique. From the suggested mechanism, high selectivity of CNT growth is achieved when a continuous layer of γ-Fe is formed on the SiO_2 layer and large clusters of $FeSi_2$ or $FeSiO_4$ are formed on the silicon surface [12]. However, a significant drawback of this technique is the high resistivity of SiO_2 layer [13], which will increase the electrical contact resistance between CNTs and Si substrate and limit its performance.

In order to achieve selective growth of CNTs on the Si surface, Labunov et al. have reported the reversible selective growth of CNTs on either Si or SiO_2 surfaces by varying the gas dynamic factors in a CVD process. In the reported outcomes, reversible selective growth of CNTs has been achieved on either Si surface or 100 nm thick SiO_2 surface, depending on the gas flow rate [14]. Besides gas dynamic factors, an important factor in determining the selectivity of CNT growth on Si/SiO_2 substrates is the growth temperature. As the selectivity of CNT growth on Si/SiO_2 substrates relies heavily on the thermo-diffusivity profile of Fe particles on the Si/SiO_2 substrates, growth temperature significantly impacts the selectivity of CNT growth [12]. In the investigations on the temperature-dependent growth of CNTs by volatile catalyst (ferrocene/xylene) source CVD technique, Sengupta et al. have reported improvements in the crystallinity of CNTs at higher synthesis temperatures [15]. At the same time, Bai et al. have reported temperature-dependent profile of CNT growth rate by changing the pyrolysis temperature in the CNT synthesis process [16]. Besides the temperature-dependent profile, Kar et al. have investigated the effect of substrate heating and microwave attenuation on the field emission properties of ferrocene-grown CNTs. From the reported work, substrate heating and microwave attenuation contribute to drastic improvement of CNT field emission current density from 200 $\mu A/cm^2$ to 14.5 mA/cm^2 [17]. Nevertheless, to realize the integration of the nanostructured field emitter in modern vacuum electronic applications, a clearer understanding of the mechanism in the temperature-dependent selective growth of CNTs on Si/SiO_2 structures is required. But there exist only limited studies on this issue. Therefore, studies on the temperature-dependent growth of CNTs on Si/SiO_2 substrates are called for.

In this study, we first perform a comparative study on the temperature-dependence of CNT growth on pristine and 2 μm SiO_2-deposited Si substrates. Selective growth of CNTs on pristine Si substrate at 790 °C is achieved. The possible mechanism of the selective growth condition is discussed. By utilizing the achieved selective growth condition, we fabricate CNT FEAs by growing CNT bundles selectively at the Si surface in fabricated SiO_2 pits at inter-pit separation distances of 4–10 μm. Field emission current density greater than 100 mA/cm^2 is obtained for all inter-pit distances. The effect of inter-pit distance on the FE properties of CNT FEAs is also explored by electrostatic simulations which further explain the experimental observations.

2. Experimental method

Carbon Nanotubes (CNTs) are grown on 2 μm SiO_2-deposited and pristine Si substrate using Chemical Vapour Deposition (CVD) with a volatile catalyst source as reported by Navitski et al. [18]. A typical CVD process is carried out in a quartz tube reactor through

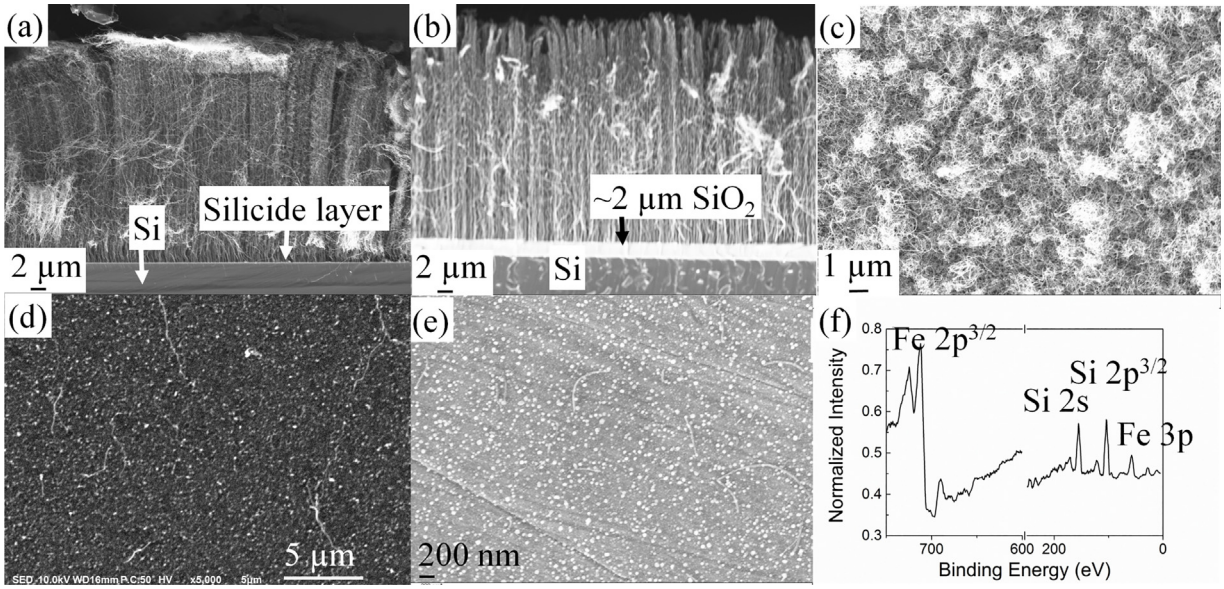

Fig. 2. SEM images: Cross sectional view of CNTs grown on (a) Si and (b) SiO_2 substrates at 860 °C growth temperature; plan view of CNTs grown on Si substrates at (c) 790 °C and (d) 860 °C growth temperatures. (e) SEM image and (f) XPS Spectra of $FeSi_2$.

which 100 sccm Argon gas flows at various temperatures of 760, 790, 800, 820, 840 860 and 880 °C, under continuous injection of ferrocene/xylene solution (1 wt% ferrocene). The growth duration is fixed at 60 s. Based on the attempted growth temperatures, selective growth of CNTs on pristine Si substrate is obtained at 790 °C. Utilizing this selective growth condition, CNT Field Emitter Arrays (FEAs) are fabricated by growing CNT bundles in pre-fabricated SiO_2 pits. The fabrication process of the SiO_2 pits is illustrated in Fig. 1, as described in a previous study by our research group [19]. To fabricate the SiO_2 pits, 2 μm of SiO_2 layer is first deposited on highly n-doped (Resistivity: 0.18 Ω com; Thickness: 300 μm) using Plasma-Enhanced Chemical Vapor Deposition (PECVD) technique. After that, the deposited SiO_2 layer is etched selectively by means of photolithography and dry etching techniques, to form SiO_2 pits of ~2 μm in diameter. By using the obtained selective growth condition of CNTs, CNT bundles are grown selectively on the exposed Si surface under the SiO_2 pits.

The morphologies of CNTs and Si/SiO_2 structure are characterized by field emission scanning electron microscopy (FESEM, LEO 1550 Gemini SEM) and transmission electron microscopy (TEM, Philips Tecnai 20). The field emission properties of the CNT FEAs are measured using a planar-anode measurement system under high vacuum condition (10^{-4} Pa). The cathode-anode distance and the effective emission area are estimated to be 18 μm and 0.75 mm^2, respectively.

3. Results and discussion

Fig. 2(a) and (b) shows the Scanning Electron Microscope (SEM) images of CNT films grown on Si and SiO_2 substrates, respectively, at 860 °C. From the SEM images, vertically aligned CNTs are formed on both Si and SiO_2 substrates at 860 °C growth temperature. It is found that CNTs show significant changes in growth orientation as the growth temperature increases from 790 to 860 °C. From Fig. 2(a), (b) and (d), CNTs show vertical alignment at a higher growth temperature of 860 °C on both Si and SiO_2 substrates. In contrast, at growth temperature of 790 °C, CNTs show a dense lateral growth, resulting in a "spaghetti-like" CNT morphology (Fig. 2(c)). The change in CNT alignment with growth temperature can be explained by the mechanisms of CNT growth and alignment [20]. Fundamentally, CNTs are grown by the diffusion of carbon feedstock into catalytic nanoclusters formed upon thermal

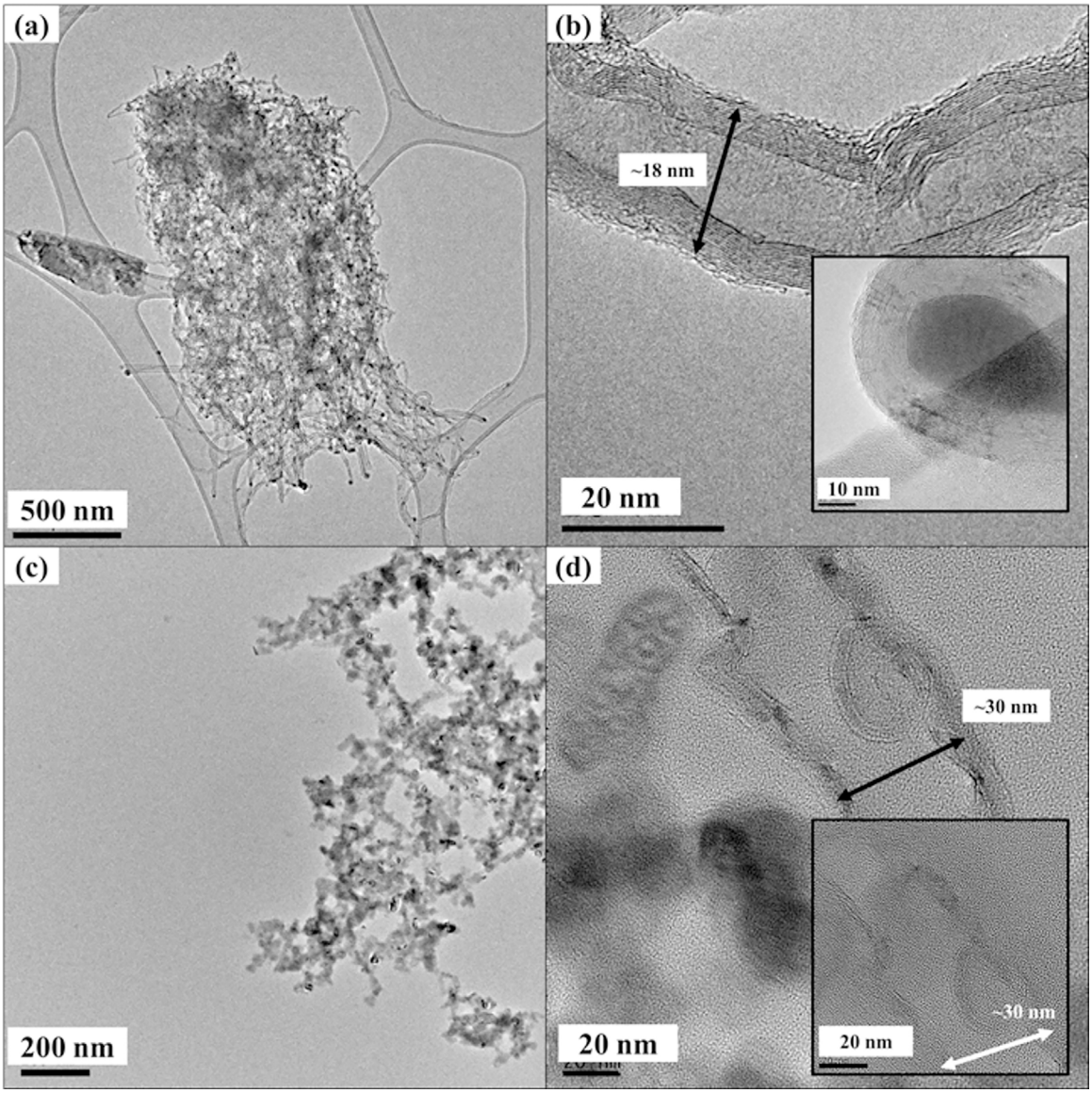

Fig. 3. TEM images of CNTs grown on (a and b) Si; and (c and d) SiO_2 substrates at growth 860 °C growth temperature.

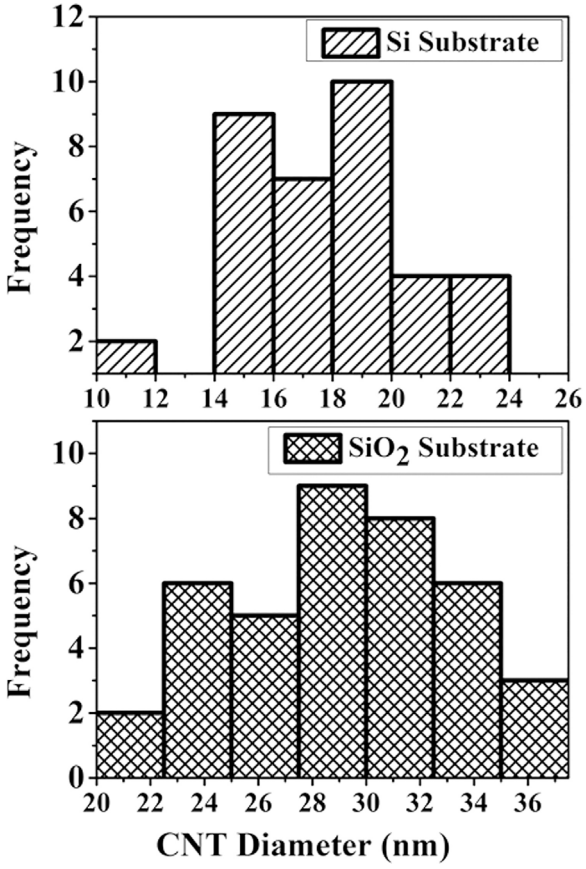

Fig. 4. CNT diameters distribution on Si and SiO_2 substrates at 860 °C growth temperature.

annealing [21]. At higher CNT growth temperatures, the catalytic nanoclusters size and distribution is small and homogeneous. The small and homogeneous catalytic particles result in the formation of densely packed CNT forest which is afflicted with high Van der Waals interaction forces between the walls of the CNTs. The high inter-CNT Van der Waals interactions give "packing" effect to the CNT film, resulting in vertical alignment. In contrast, lower CNT growth temperatures lead to the formation of relatively larger nanoclusters, resulting in weaker inter-CNT Van der Waals interaction and hence lateral growth of CNTs [22].

Besides the morphological properties of CNTs, we have observed a conductive barrier layer formed at the CNT-Si interface, as shown in Fig. 2(a). For further investigation on the CNT-Si interface, we removed the CNTs on the bare Si substrate with tweezer to reveal the underneath silicide layer. The SEM image and the X-ray Photoelectron Spectroscopy (XPS) spectra of the thin layer are shown in Fig. 2(e) and (f). From Fig. 2(e), the formation of individual clusters on the Si substrate shows similar morphological characteristics to a $FeSi_2$ layer, as reported by Dahal et al. [23]. For further justification, we have performed XPS analysis on the silicide layer. As shown in Fig. 2(f), $FeSi_2$ peaks are formed at the binding energies of 54.64 and 707 eV, indicating the 2p and 3p hybridization of $FeSi_2$. The formation of $FeSi_2$ hybridization peaks suggests the formation of iron silicide, which agrees well with the reported findings by Ohtsu et al. [24]. The formation of $FeSi_2$ layer during ferrocene/xylene pyrolysis agrees well with Jung et al., where ferrocene will first be thermally-decomposed to continuously deposit Fe particles onto the Si substrate. Fe particles will then first diffuse into the Si substrate to form a continuous $FeSi_2$ barrier layer. When the barrier layer is formed, the subsequent Fe particles deposited on the substrate will be "blocked" from further

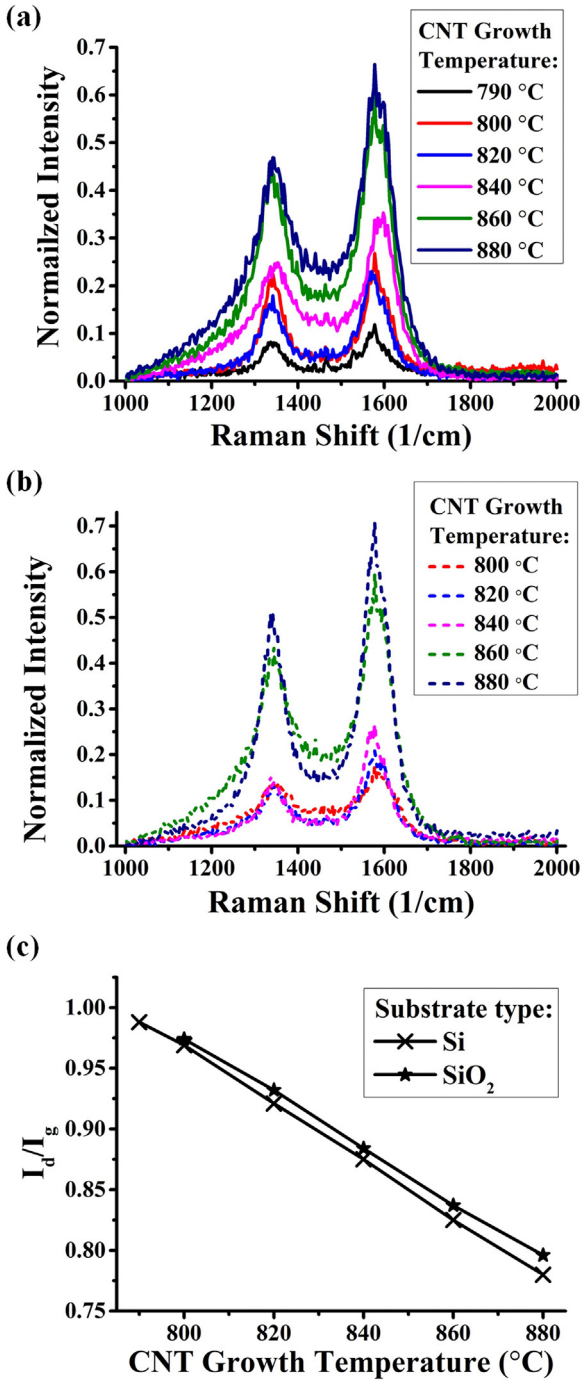

Fig. 5. Raman spectroscopy of CNTs grown on (a) Si, and (b) SiO_2 substrates; (c) I_d/I_g ratios of CNTs grown on Si and SiO_2 substrates.

diffusion into Si substrate, hence forming catalytic nanoclusters for CNT growth [12].

To further investigate the morphological properties of CNTs, we have performed Transmission Electron Microscopy (TEM) imaging on CNTs grown on Si and SiO_2 substrates. As shown in Fig. 3, tubular structure of CNTs is observed on both Si and SiO_2 substrates, similar to the CNT morphology reported by Kar et al. [17]. Multi-Walled CNT structure with diameter of ~18 nm and ~30 nm can be observed on both Si and SiO_2 substrates. From Fig. 3(d), it can be seen that CNTs grown on SiO_2 substrate show higher irregularity in CNT walls as compared to those grown on Si substrate, which possibly indicate the higher defectiveness of CNTs

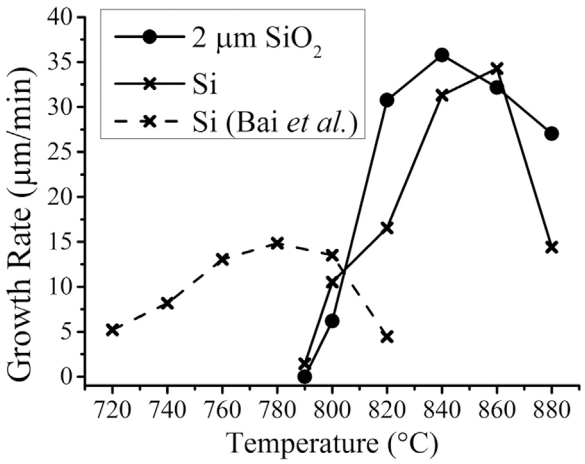

Fig. 6. CNT growth rate on Si and SiO_2 surfaces; CNT growth rate reported by Bai et al. on Si surface, at different growth temperatures [16].

grown on SiO_2 substrates. From the CNT clusters shown in Fig. 3(a) and (c), a detailed quantitative study on the CNT diameters grown on both Si and SiO_2 substrates is carried out, as shown in Fig. 4. From the quantitative study, CNTs grown on SiO_2 substrate show larger average diameter of 29 nm as compared to 18 nm on Si substrate. The larger diameter of CNTs grown on SiO_2 substrate suggests the formation of larger catalytic nanoclusters during the pyrolysis process [25]. Generally, CNT growth on Si/SiO_2 substrate using ferrocene/xylene catalyst will be initiated upon formation of continuous barrier layer on the surface of the substrate via thermal diffusion of Fe particles [12]. The formation of barrier layer on the substrates relies significantly on the thermal diffusivity and the solubility of Fe particles in the substrate [26]. According to the reported literature, Fe particles possess lower solid diffusivity on SiO_2 substrate as compared to Si [27,28]. Therefore, in the same CVD process, less Fe particles are anticipated to diffuse into the SiO_2 substrate as compared to that into Si substrate, causing more Fe particles to precipitate on the surface of the SiO_2 substrate. This causes the formation of larger catalytic nanoclusters, which leads to the formation of CNTs with larger diameters.

To further investigate the structural properties of CNTs, we have performed Raman Spectroscopy studies on CNTs grown on Si and SiO_2 layers (Fig. 5). The appearance of D-band (1339–1444 cm^{-1}) and G-band (1575–1577 cm^{-1}) in the Raman spectrum for all investigated CNT samples indicate the presence of disorder in the graphitic structure [29] and the in-plane vibration of C—C bond [30]. Generally, CNTs show decreasing I_d/I_g ratio, indicating the improvement in crystallinity, as the growth temperature increases. This agrees well with Lee et al. where the degree of crystalline perfection in CNTs increases progressively as the growth temperature increases [31]. From Fig. 5(c), it is shown that the I_d/I_g ratios of CNTs grown on Si and SiO_2 substrates are similar at 800–880 °C growth temperatures. The slightly higher I_d/I_g ratio of CNTs grown on SiO_2 substrates can be attributed to the higher irregularity in the CNT walls, as shown in Fig. 3.

The respective CNT growth rates on Si and SiO_2 substrates at various growth temperatures are shown in Fig. 6. We also compare our experimental data on the CNT growth rate at various temperatures with that reported by Bai et al. [16]. Generally, the variation of CNT growth rate with temperature shows similar trend, with the growth rate reaching a maximum value at an optimum growth temperature, and reducing as the temperature increases further. The difference in the optimum temperature and CNT growth can be caused by the difference in ferrocene/xylene concentration and gas feedstock rate [14]. From 800 to 860 °C, the CNT growth rate on Si increases from 10.51 to 34.28 μm/min and decreases to 14.4 μm/min as the growth temperature further increases to 880 °C. At the same time, CNT growth rate on SiO_2 increases from 6.18 to 35.77 μm/min from 800 to 840 °C and decreases to 27.04 μm/min as the growth temperature increases to 880 °C. This improvement in the growth rate at higher temperature can be attributed to the higher decomposition rate of ferrocene which increases the catalytic effect of ferrocene [32]. On the other hand, the reduction of growth rate when the temperature increases beyond the optimum value can be attributed to the passivation of the Fe clusters, where hydrocarbon precursors precipitate on the catalyst particles and reduce its catalytic activity [16]. No CNT growth is observed at 760 °C on both Si and SiO_2 surfaces. But at 790 °C, while no significant CNT growth is observed on SiO_2 surface, the CNT height of ~1.25 μm is observed on Si surface.

From the obtained selective growth condition, we have speculated the mechanism of the selective growth of CNTs on Si layer, as illustrated in Fig. 7. Fundamentally, to enable CNT growth, a continuous silicide layer is required to form as a barrier layer for CNT growth [12,11]. Therefore, the selectivity of CNT growth largely

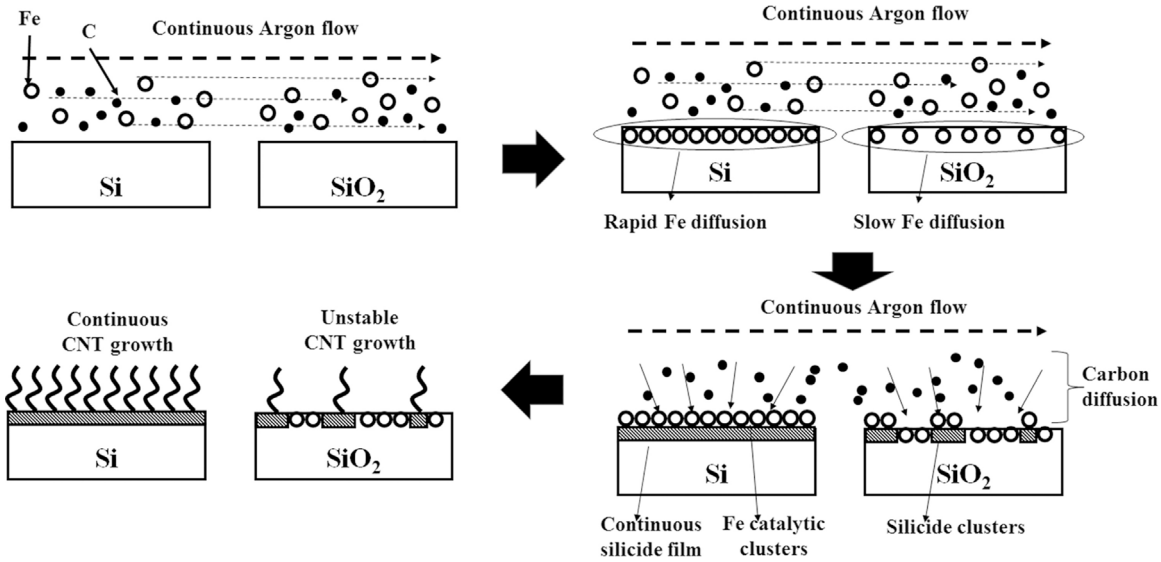

Fig. 7. Mechanism of the selective growth of CNTs on Si substrates.

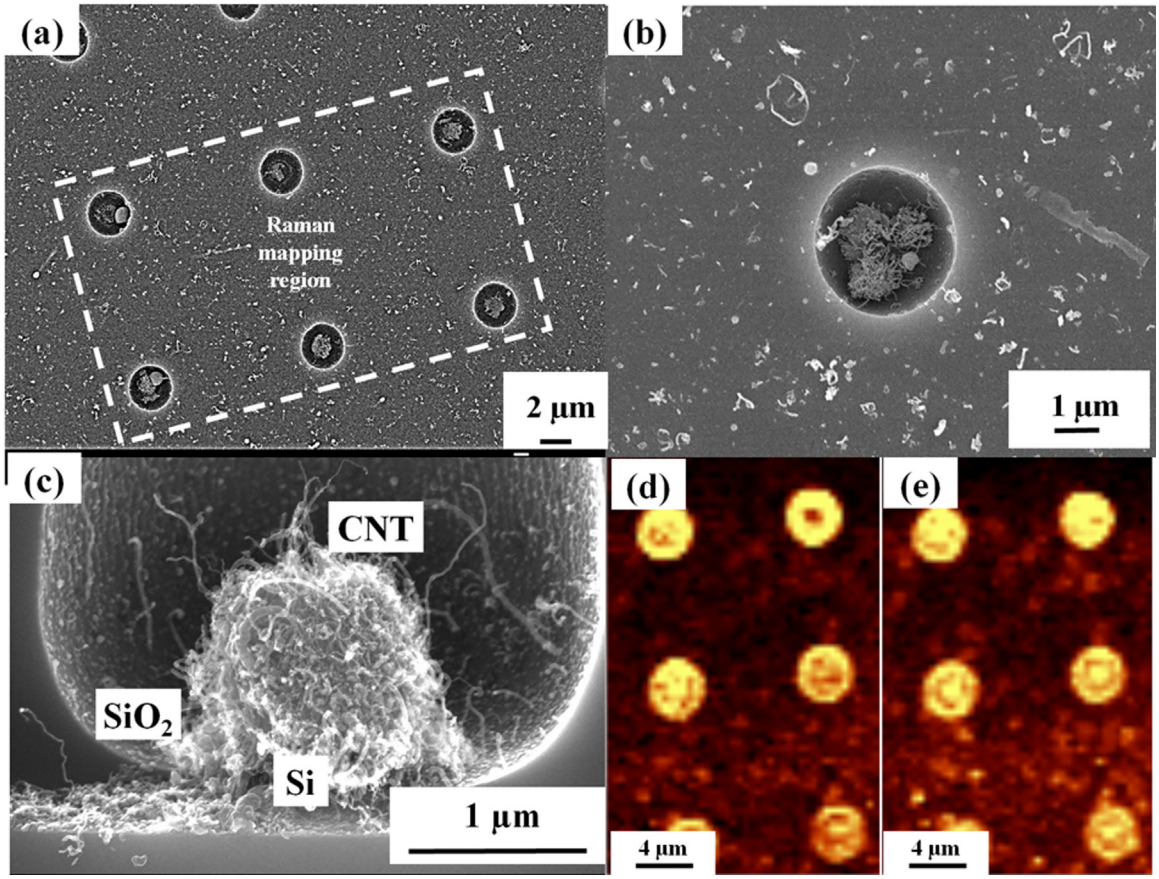

Fig. 8. SEM Images: (a): Plane view of CNT FEA; (b) plane view, and (c): cross-sectional view of single CNT bundle. Raman map: (d) 1339–1444 cm^{-1}(D-band) and (e) 1575–1577 cm^{-1} (G-band).

depends on the Fe-adsorption stage on the surface [14]. At the same time, the Fe-adsorption on the surface heavily relies on the thermal diffusivity of Fe on the target surface [33]. From the reported studies, the diffusivity of Fe on Si ($\sim 10^{-6}$ cm^2/s) [28] is significantly higher than on SiO_2 surface ($\sim 10^{-14}$ cm^2/s) [27] at the obtained selective growth temperature (790 °C). Furthermore, PECVD-grown SiO_2 possesses high porosity (~41%) [34], which allows more Fe particles to diffuse into the SiO_2 layer. Based on the low diffusivity and high porosity of SiO_2, it can be speculated that Fe diffuses rapidly into the Si surface during the CNT growth process, and forms a continuous layer of silicide barrier layer which favours the CNT growth. On the other hand, the lower diffusivity of Fe on SiO_2 surface hinders the formation of a continuous silicide layer within the short (60s) CNT growth duration. Therefore, at the obtained selective growth temperature, continuous silicide layers are formed on Si surfaces, whereas isolated clusters of silicide are formed on SiO_2 surface. As a result, continuous CNT growth occurs on Si layers; whereas unstable CNT growth is found on SiO_2. As the temperature increases, Fe diffusivity on both Si and SiO_2 substrates increase significantly. At higher Fe diffusivity, Fe particles obtain sufficient thermal energy to diffuse into SiO_2 surface for silicide formation which favours CNT growth. At the lower growth temperature of 760 °C, the Fe diffusivity in Si and SiO_2 reduces, which hinders the formation of continuous silicide layer. This explains the absence of CNTs on both Si and SiO_2 surfaces at growth temperature of 760 °C. Nevertheless, the precise mechanism of the selective growth remains unclear since the formation of the silicide phase on both Si and SiO_2 surfaces is not fully understood and requires further investigation.

By utilizing the obtained selective growth condition of CNTs, we next demonstrate its application in the fabrication of CNT Field Emitter Array (FEA). CNT bundles are grown selectively at 790 °C on the Si surfaces of pre-fabricated SiO_2 pits on a Si substrate. The SEM images of the fabricated CNT FEA are shown in Fig. 8. As shown in Fig. 8(a), array of pits with ~2 μm in diameter is formed in the SiO_2 layer. From Fig. 8(b), unstable growth of CNTs is found on the SiO2 layer, as agreed by the speculated mechanism discussed in Fig. 7. As shown in Fig. 8(c), entangled CNTs can be clearly observed where a randomly aligned CNT bundle of ~1.25 μm high CNTs is grown selectively at the bottom of the SiO_2 pit. To further justify the selective growth of CNTs on the Si layer, we have performed Raman mapping on the CNT FEA, as shown in Fig. 8(d) and (e). Exceptionally high intensities of D-band 1339–1444 cm^{-1}) and G-band (1575–1577 cm^{-1}) are obtained from the SiO_2 pits regions; whereas low intensities are obtained from the SiO_2 surfaces. The low intensities of D- and G-bands from the SiO_2 surface can be due to the formation of amorphous carbon and unstable growth of CNTs on the SiO_2 surface [35]. On the other hand, the exceptionally high intensities of D- and G-bands on the SiO_2 pits regions indicate the selective growth of CNTs on the Si surfaces of the FEA.

The Field Emission (FE) properties of the CNT FEAs are measured for various separation distances between SiO_2 pits and are shown in Fig. 9(a). FE current density above 100 mA/cm^2 is obtained for the investigated separation distances. For the sake of comparison, we have replotted the FE measurements obtained in this study with the reported CNT FEA with different heights reported in the literature, as shown in Fig. 9(b). The CNT heights and their respective FE performances are summarized in Table 1.

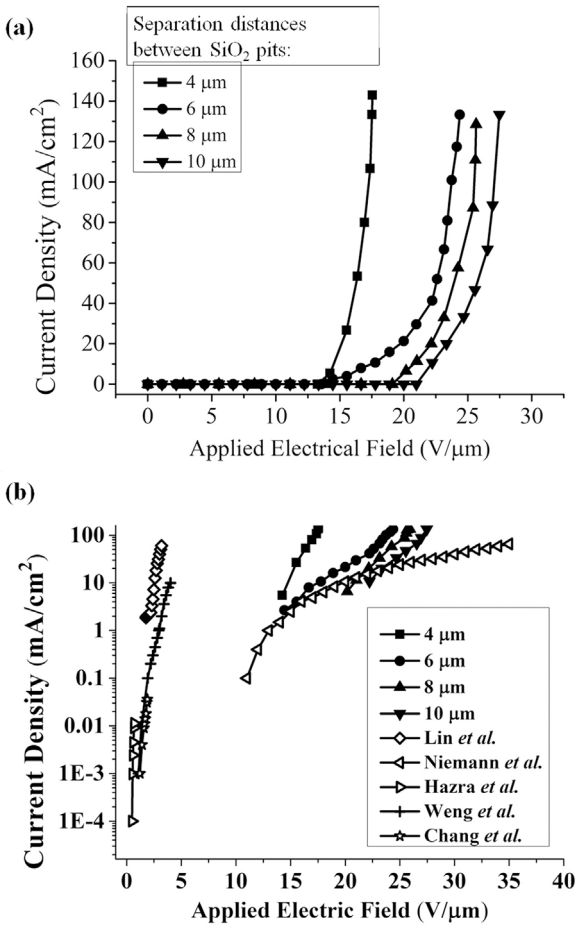

Fig. 9. (a) FE Properties of the CNT FEA at different inter-pit separation distances, (b) Comparison of the FE properties obtained in this study with the reported studies [20,36–39].

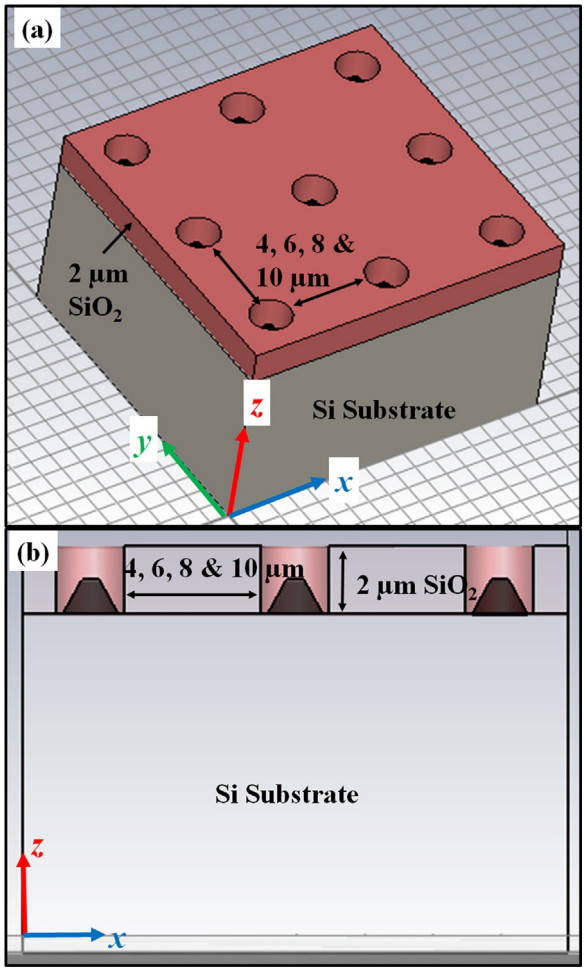

Fig. 10. (a) Orthogonal and (b) Sectional view of the CNT FEA model for simulation of the electrostatic field.

From the comparison, it is shown that the FE properties of CNTs obtained from this study compares favourably with the reported studies, achieving highest FE current density among the investigated literatures.

From the obtained FE properties (Fig. 9), the emission current density is seen to reduce as the SiO_2 pits are fabricated farther apart. This can be explained by the screening effect phenomenon of CNT FEA. It has been widely reported that the optimal separation distance between CNT for the minimization of screening effect can be expressed as R/H = 2, where R and H represent the separation distance between adjacent CNT pillars and CNT height, respectively [40]. For inter-SiO_2 pits separation distances of 4, 6, 8 and 10 μm, the R/H > 2 condition holds, suggesting the minimization of screening effect between CNT bundles for all these separation distances [38]. Then, larger inter-SiO_2 pits separation distances simply correspond to the presence of fewer CNTs per unit area, which results in lower FE current density. But the reported optimal condition R/H = 2 was computed based on CNT pillars which possess a cylindrical geometry [40], different from the approximate-conical shape CNT bundles obtained in the present study. For further investigation, we have simulated the electrostatic field distribution for the CNT bundles at inter-pit separation distances of 4, 6, 8 and 10 μm using CST EM Studio (https://www.cst.com/products/cstems). To better resemble the geometrical shape of the obtained CNT bundles, we have made an approximate model which represents the shape of the CNT bundles obtained, as shown in Fig. 10.

Fig. 11(a) shows the sectional view of the simulated electric field distribution of the CNT FEA at 4 μm inter-pit separation distance,

Table 1
Compilation of the FE current densities obtained in this study with the reported studies.

CNT Field Emitter	CNT Height	Current Density @ Applied Electric Field
This work – 4 μm separation	~1.25 μm	17.55 V/μm @ 142.93 mA/cm^2
This work – 6 μm separation		24.38 V/μm @ 133.33 mA/cm^2
This work – 8 μm separation		25.93 V/μm @ 133.33 mA/cm^2
This work – 10 μm separation		27.46 V/μm @ 133.33 mA/cm^2
Lin et al. [36]	0.8 μm	3.2 V/μm @ 60 mA/cm^2
Niemann et al. [20]	10 μm	35 V/μm @ 65.3 mA/cm^2
Weng et al. [37]	10 μm	4 V/μm @ 10 mA/cm^2
Chang et al. [38]	15 μm	2 V/μm @ 36 mA/cm^2
Hazra et al. [39]	50 μm	0.7 V/μm @ 11 mA/cm^2

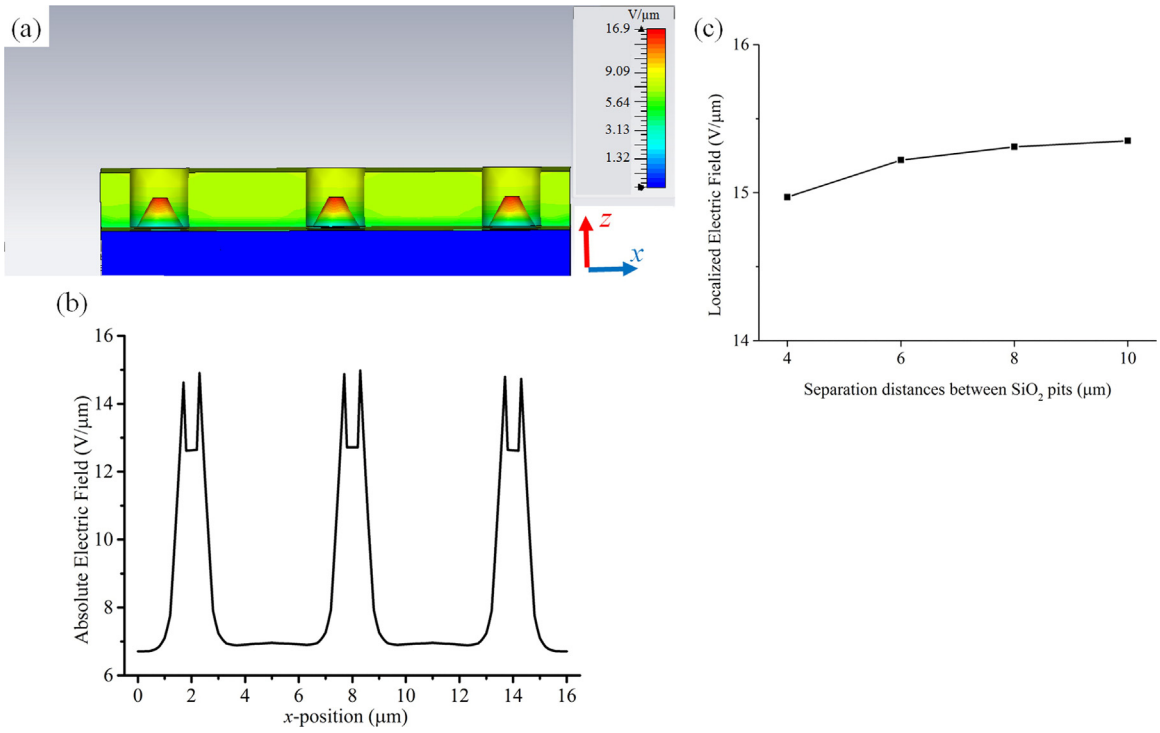

Fig. 11. (a) Sectional view of the simulated electric field distribution for the CNT FEA model; (b) variation of the simulated electric field on the CNT tips along x-direction; (c) localized electric field on the edges of the CNT bundle tips at various separation distances between SiO_2 pits.

where different colours denote different electric field intensities. It can be clearly seen from the Fig. 11(a) that localized electric field enhancement occurs on the tips of the CNT bundles. Since the electric field distribution for CNT bundles is similar at 4–10 μm inter-SiO_2 pit separation distances for a given applied electric field, we only show the electric field distribution for the CNT FEA with inter-pit distance of 4 μm. For a numerical assessment, the simulated electric field distribution on the CNT tips is shown in Fig. 11(b). It can be observed that the electric field for the CNT bundles is much higher at the edge (about 15 V/μm) than at the centre (about 12.7 V/μm). To investigate the influence of inter-pit separation distance on the electric field, we have plotted the simulated electric field on the edge of CNT bundles for different separation distances as shown in Fig. 11(c). The simulated localized electric field on the edge of CNT bundles shows insignificant increment (from 15 to 15.35 V/μm, ~2% increment) when the separation distance increases from 4 to 10 μm. Thus, the only reason for lower FE current density is the presence of fewer CNTs per unit area as the separation between SiO_2 pits increases.

4. Conclusion

A comparative study has been carried out to investigate the CNT growth rates on Si and SiO_2 substrates using ferrocene/xylene catalyst source at various growth temperatures. Selective growth of CNT has been achieved on Si surface at the growth temperature of 790 °C. The selectivity of CNT growth can be attributed to the difference in thermal diffusivity of Fe between Si and SiO_2 substrates under similar solid solubility, resulting in selective formation of continuous $FeSi_2$ phase on Si surface. Utilizing the obtained selective growth condition, CNT field emitter arrays (FEAs) have been fabricated by growing CNT bundles selectively in pre-fabricated SiO_2 pits with inter-pit separation distances varying from 4 to 10 μm. Field emission current density greater than 100 mA/cm^2 has been obtained for all separation distances. From the simulated electric field distribution, it has been found that the localized electric field on CNT tips is similar for all separation distances due to the fulfilment of $R/H > 2$ condition. These results together demonstrate that CNTs can be selectively grown on Si surface of a pre-fabricated Si/SiO_2 structure by adjusting the growth temperature for field emitter array applications.

Acknowledgement

This work has been supported by the Office for Space Technology and Industry (OSTIn), Singapore, under the project S14-1126-NRF OSTIn-SRP.

References

[1] D. Bishop, Nanotechnology and the end of Moore's Law? Bell Syst. Tech. J. 10 (2005) 23–28, doi:http://dx.doi.org/10.1002/bltj.20117.
[2] H. Iwai, End of the scaling theory and Moore's law, 16th Int. Work. Junction Technol. 2016 (2016) 1–4, doi:http://dx.doi.org/10.1109/IWJT.2016.7486661.
[3] J. Han, M. Meyyappan, The device made of nothing, IEEE Spectr. 51 (2014) 30–35, doi:http://dx.doi.org/10.1109/MSPEC.2014.6840798.
[4] J.H. Bala, R.J. Barker, Introduction and overview, Mod. Microw. Millimeter-Wave Power Electron, (2003), pp. 1–33, doi:http://dx.doi.org/10.1007/978-3-0348-8965-0_1 http://link.springer.com/chapter/ (Accessed 29 December 2014).
[5] K. Panda, K.J. Sankaran, B.K. Panigrahi, N.H. Tai, I.N. Lin, Direct observation and mechanism for enhanced electron emission in hydrogen plasma-treated diamond nanowire films, ACS Appl. Mater. Interfaces 6 (2014) 8531–8541, doi:http://dx.doi.org/10.1021/am501398s.
[6] Y. Zhang, C. Wu, Y. Zheng, T. Guo, Synthesis and efficient field emission characteristics of patterned ZnO nanowires, J. Semicond. 33 (2012) 23001, doi:http://dx.doi.org/10.1088/1674-4926/33/2/023001.
[7] A.K. Samantara, D.K. Mishra, S.R. Suryawanshi, M.A. More, R. Thapa, D.J. Late, B. K. Jena, C.S. Rout, Facile synthesis of Ag nanowire-rGO composites and their promising field emission performance, RSC Adv. 5 (2015) 41887–41893, doi:http://dx.doi.org/10.1039/C5RA00308C.
[8] W.I. Milne, K.B.K. Teo, G.A.J. Amaratunga, P. Legagneux, L. Gangloff, J.-P. Schnell, V. Semet, V. Thien Binh, O. Groening, Carbon nanotubes as field emission sources, J. Mater. Chem. 14 (2004) 933, doi:http://dx.doi.org/10.1039/b314155c.
[9] M. Khaneja, S. Ghosh, S. Gautam, P. Kumar, J.S. Rawat, P.K. Chaudhury, V.D. Vankar, V. Kumar, High field emission current density from patterned carbon nanotube field emitter arrays with random growth, J. Nanosci. Nanotechnol. 15 (2015) 3846–3851, doi:http://dx.doi.org/10.1166/jnn.2015.9507.

[10] S. Handuja, S.P. Singh, P. Srivastava, V.D. Vankar, Growth of long aligned carbon nanotubes on amorphous hydrogenated silicon nitride by thermal chemical vapor deposition, Mater. Lett. 63 (2009) 1249–1251, doi:http://dx.doi.org/10.1016/j.matlet.2009.02.050.
[11] Z. Zhang, Y.A. Zhou, Y. Yue, Growth carbon nanotubes directly on pristine silicon substrates, Int. J. Nanosci. 5 (2006) 433–439.
[12] Y.J. Jung, B. Wei, R. Vajtai, P.M. Ajayan, Mechanism of selective growth of carbon nanotubes on SiO 2/Si patterns, Nano Lett. 3 (2003) 2–5, doi:http://dx.doi.org/10.1021/nl034075n.
[13] W.K. Choi, C.K. Choo, Y.F. Lu, Electrical characterization of rapid thermal annealed radio frequency sputtered silicon oxide films, J. Appl. Phys. 80 (1996) 5837, doi:http://dx.doi.org/10.1063/1.363576.
[14] V.A. Labunov, B.G. Shulitski, A.L. Prudnikava, Y.P. Shaman, A.S. Basaev, The effect of gas-dynamic factors on selective carbon-nanotube synthesis by injection CVD method for field-emission cathodes, J. Soc. Inf. Disp. 17 (2009) 489–495, doi:http://dx.doi.org/10.1889/jsid17.5.489.
[15] J. Sengupta, A. Jana, N.D. Pradeep Singh, C. Jacob, Effect of growth temperature on the CVD grown Fe filled multi-walled carbon nanotubes using a modified photoresist, Mater. Res. Bull. 45 (2010) 1189–1193, doi:http://dx.doi.org/10.1016/j.materresbull.2010.05.017.
[16] X. Bai, D. Li, Y. Wang, J. Liang, Effects of temperature and catalyst concentration on the growth of aligned carbon nanotubes, Tsinghua Sci. Technol. 10 (2005) 729–735, doi:http://dx.doi.org/10.1016/S1007-0214(05)70142-5.
[17] R. Kar, S.G. Sarkar, C.B. Basak, A. Patsha, S. Dhara, C. Ghosh, D. Ramachandran, N. Chand, S.S. Chopade, D.S. Patil, Effect of substrate heating and microwave attenuation on the catalyst free growth and field emission of carbon nanotubes, Carbon N. Y. 94 (2015) 256–265, doi:http://dx.doi.org/10.1016/j.carbon.2015.07.002.
[18] A.L. Prudnikava, B.G. Shulitski, V.A. Labunov, A. Navitski, V. Sakharuk, G. Müller, Efficient high-current field emission from arrays of CNT columns, Tech. Dig. – 2009 22nd Int. Vac. Nanoelectron. Conf. IVNC 2009 (2009) 257–258, doi:http://dx.doi.org/10.1109/IVNC.2009.5271645.
[19] Y.D. Lim, A. Avramchuck, D. Grapov, B.K. Tay, A. Sheel, V. Labunov, Field emission characteristics of short CNT bundles, Int Vac. Electron. Conf., IEEE, Monteray, California, 2016.
[20] D.L. Niemann, J. Silan, J.L. Killian, K.R. Schwanfelder, M. Rahman, M. Meyyappan, C.V. Nguyen, Carbon nanotube field emission devices with integrated gate for high current applications, 2008 8th IEEE Conf. Nanotechnol. (2008) 456–459, doi:http://dx.doi.org/10.1109/NANO.2008.139.
[21] M. Meyyappan, L. Delzeit, A. Cassell, D. Hash, Carbon nanotube growth by PECVD: a review, Plasma Sources Sci. Technol. 12 (2003) 205–216, doi:http://dx.doi.org/10.1088/0963-0252/12/2/312.
[22] A. Ramirez, N. Latorre, R. Mallada, R.M. Tiggelaar, A. Monzón, Unraveling the growth of vertically aligned carbon nanotubes by chemical vapor deposition, Mater. Res. Express. 45604 (2013), doi:http://dx.doi.org/10.1088/2053-1591/1/4/045604.
[23] N. Dahal, V. Chikan, Phase-controlled synthesis of iron silicide (Fe3Si and FeSi 2) nanoparticles in solution, Chem. Mater. 22 (2010) 2892–2897, doi:http://dx.doi.org/10.1021/cm100224b.
[24] N. Ohtsu, M. Oku, K. Satoh, K. Wagatsuma, Dependence of core-level XPS spectra on iron silicide phase, Appl. Surf. Sci. 264 (2013) 219–224, doi:http://dx.doi.org/10.1016/j.apsusc.2012.09.176.
[25] C.L. Cheung, A. Kurtz, H. Park, C.M. Lieber, Diameter-controlled synthesis of carbon nanotubes, J. Phys. Chem. B 106 (2002) 2429–2433, doi:http://dx.doi.org/10.1021/jp0142278.
[26] S. Handuja, P. Srivastava, V.D. Vankar, On the growth and microstructure of carbon nanotubes grown by thermal chemical vapor deposition, Nanoscale Res. Lett. 5 (2010) 1211–1216, doi:http://dx.doi.org/10.1007/s11671-010-9628-8.
[27] J.D. McBrayer, Diffusion of metals in silicon dioxide, J. Electrochem. Soc. 133 (1986) 1242, doi:http://dx.doi.org/10.1149/1.2108827.
[28] A.A. Istratov, H. Hieslmair, E.R. Weber, Iron and its complexes in silicon, Appl. Phys. A Mater. Sci. Process. 69 (1999) 13–44, doi:http://dx.doi.org/10.1007/s003390050968.
[29] M.S. Dresselhaus, A. Jorio, M. Hofmann, G. Dresselhaus, R. Saito, Perspectives on carbon nanotubes and graphene Raman spectroscopy, Nano Lett. 10 (2010) 751–758, doi:http://dx.doi.org/10.1021/nl904286r.
[30] M. a Pimenta, G. Dresselhaus, M.S. Dresselhaus, L.G. Cançado, a Jorio, R. Saito, Studying disorder in graphite-based systems by Raman spectroscopy, Phys. Chem. Chem. Phys. 9 (2007) 1276–1291, doi:http://dx.doi.org/10.1039/b613962k.
[31] C.J. Lee, J. Park, Y. Huh, J. Yong Lee, Temperature effect on the growth of carbon nanotubes using thermal chemical vapor deposition, Chem. Phys. Lett. 343 (2001) 33–38, doi:http://dx.doi.org/10.1016/S0009-2614(01)00680-7.
[32] F.A. Rabbani, Z.O. Malaibari, M.A. Atieh, A. Jamie, Catalytic synthesis of substrate-free, aligned and tailored high aspect ratio multiwall carbon nanotubes in an ultrasonic atomization head CVD reactor, J. Nanomater. (2016) 2016, doi:http://dx.doi.org/10.1155/2016/4189456.
[33] S.V. Koveshnikov, G.A. Rozgonyi, Iron diffusivity in silicon: impact of charge state, Appl. Phys. Lett. 860 (1995) 860, doi:http://dx.doi.org/10.1063/1.113411.
[34] P. Yang, L. Liu, J. Mo, W. Yang, Characterization of PECVD grown porous SiO2 thin films with potential application in an uncooled infrared detector, Semicond. Sci. Technol. 25 (2010) 45017, doi:http://dx.doi.org/10.1088/0268-1242/25/4/045017.
[35] H. Liang, L. Delian, C. Xian, Y. Li, Z. Yuqing, The deposition of a thick tetrahedral amorphous carbon film by argon ion bombardment, Appl. Surf. Sci. 258 (2012) 4794–4800, doi:http://dx.doi.org/10.1016/j.apsusc.2012.01.100.
[36] K.-C. Lin, H.-W. Chen, C.-P. Juan, R.-L. Lai, Y.-Y. Hsu, H.-C. Cheng, Carbon-nanotube-based field emission devices with a self-focusing gate structure, J. Electrochem. Soc. 155 (2008), doi:http://dx.doi.org/10.1149/1.2826228 K38.
[37] T.W. Weng, Y.H. Lai, K.Y. Lee, Area effect of patterned carbon nanotube bundle on field electron emission characteristics, Appl. Surf. Sci. 254 (2008) 7755–7758, doi:http://dx.doi.org/10.1016/j.apsusc.2008.02.020.
[38] C.T. Chang, C.P. Juan, H.C. Cheng, Pillar height dependence of field-emission properties in an array of carbon nanotube pillars, Jpn. J. Appl. Phys. 52 (2013) 3–8, doi:http://dx.doi.org/10.7567/JJAP.52.085101.
[39] K.S. Hazra, T. Gigras, D.S. Misra, Tailoring the electrostatic screening effect during field emission from hollow multiwalled carbon nanotube pillars, Appl. Phys. Lett. 98 (2011) 123116, doi:http://dx.doi.org/10.1063/1.3565243.
[40] G. Bocharov, A. Eletskii, Theory of carbon nanotube (CNT)-based electron field emitters, Nanomaterials 3 (2013) 393–442, doi:http://dx.doi.org/10.3390/nano3030393.